Transactions of the Korean Society of Mechanical Engineers Vol. 7, No. 1, pp. 73~82, 1983.

<Original>

Dynamic Stability of Orthotropic Cylindrical Shells under Axial Compression

Chon Wook Kim* and Sung Y. Lu**

(Received September 15, 1982)

壓縮荷重을 받는 直交異方性 圓筒셸의 動的 安定性

金 天 旭 · Sung Y. Lu

抄 錄

初期缺陷을 가진 直交異方性圓筒셸이 軸方向스텝荷重을 받은 때의 動的挫屈을 연구하였다. 圓筒셸의 運動方程式은 非線型 Donnell 方程式을 사용하였으며 變位式에는 6個項을 채용하였다. 挫屈條件은 圓筒셸의 垂直變位와 진이變化의 급격한 變化로써 정의하였다. 挫屈모우드形狀은 初期缺陷과 셸材料의 異方性에 따라 달라짐을 발견하였고 挫屈强度는 初期缺陷의 증가에 따라 크게 감소된다.

1. Introduction

Numerous static stability analyses have been made of isotropic shells. When a cylindrical shell is under axial compression, the small deflection theory predicts buckling stresses always higher than those found by experiments. This discrepancy was studied by many authors. Large normal deflection patterned in diamond shape was first advanced by von Karman and Tsien [1]. The postbuckling analysis made by them was based on the Rayleigh-Ritz method and nonlinear strain-displacement relations. Several authors have discussed the dependence of computed buckling load on the form of the assumed deflection function. Another suggestion that has been made to explain the lower buckling strength found from tests is that the initial shape of the cylinder deviates slightly from a perfect circular cross-section. The effect of imperfections on the stability of a cylindrical shell under axial compression was studied by Donnell and Wan [2] in 1950.

The load-carrying capacity of the shell structure can be effectively increased by using stiffening elements or fibrous composites which are essentially orthotropic. Proper selection of the orthotropic properties can also lessen the effect of imperfection on the stability of the shell. Static analyses of orthotropic cylinders have been made by Khot [3] and by Booton and Tennyson [4] recently.

The study of dynamic stability of shell structures has been a subject of interest since 1960. Roth and Klosner [5] studied the dynamic stability of long, circular cylindrical shells having initial imperfections subjected to

* Department of Mechanical Engineering, Yonsei University, Seoul, Korea

** Department of Engineering Sciences, University of Florida, Gainesville Florida, 32611

time-dependent axial edge loads. Their analysis showed that the dynamic buckling load for a perfect cylindrical shell subjected to a step loading was almost same as the classical static buckling load and also that the initial imperfections played a dominant role in the reduction of critical stress. In 1975, Tamura and Babcock [6] also investigated the dynamic stability of an imperfect circular cylindrical shell subjected to a step loading in the axial direction. In their analysis, the effect of axial inertia was included in an approximate manner and a significant reduction of dynamic buckling loads compared to perfect shell was observed. Recently, Zimcik and Tennyson [7] presented a study on the stability of circular cylindrical shells under transient axial impulsive loading and compared their numerical results with experimental data. Studies reported in [5, 6, 7] deal with isotropic cylinders.

In the present study the dynamic buckling of an orthotropic circular cylindrical shell under an axial step load is investigated using the nonlinear Donnell-type shell equations of motion. Instead of attempting to solve the equations directly, an approximate six-term deflection function having time-dependent coefficients is assumed. After integration by Galerkin's method, six coupled, second-order ordinary differential equations are obtained. A numerical integration method is applied to solve these equations as a function of seven parameters which are related to loading, imperfection, geometry and orthotropy. A buckling criterion is defined with regards to the sudden increase of end-shortening and normal deflection. The buckling mode shapes are found to change with initial imperfections and material orthotropy. The effect of initial imperfection on the stability is significant. A comparison with some available experimental results is made.

2. Formulation

The nonlinear equations of motion are based on the Donnell-type theory which is valid for cylinders of moderate length. In the formulation of these equations we assume: (a) large displacement in the normal direction, and (b) longitudinal and tangential inertia terms negligible.

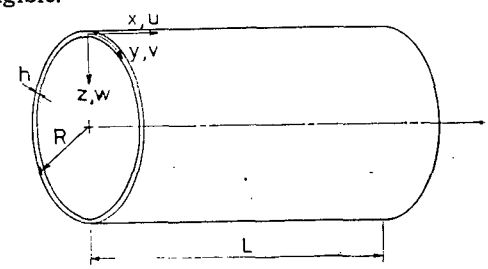

Fig. 1 Circular cylindrical shell.

Figure 1 shows the cylindrical shell geometry and coordinate system. Let (u, v) represent the displacement of components of a point on the mid-surface in the direction of the cylindrical coordinate axes (x, y) in the axial and circumferential directions, respectively and w is displacement in the inward normal z direction. Also, the stress and strain components are denoted by $(\sigma_x, \sigma_y, \tau_{xy})$ and $(\varepsilon_x, \varepsilon_y, \gamma_{xy})$, respectively.

Assume that the orthotropic symmetry axes of the material coincide with the coordinate directions, so that the in-plane stress strain relations may be written as

$$\begin{Bmatrix}\sigma_x\\ \sigma_y\\ \tau_{xy}\end{Bmatrix}=\frac{1}{1-\nu_{xy}\nu_{yx}}\begin{bmatrix}E_x & \nu_{xy}E_y & 0\\ \nu_{yx}E_x & E_y & 0\\ 0 & 0 & (1-\nu_{xy}\nu_{yx})G_{xy}\end{bmatrix}\begin{Bmatrix}\varepsilon_x\\ \varepsilon_y\\ \gamma_{xy}\end{Bmatrix} \tag{1}$$

where E_x, E_y and G_{xy} denote Young's moduli in the x- and y-directions and shear modulus,

respectively; ν_{xy} represents the relative contraction in the y-direction influenced by the tension in the x-direction. It is noted that

$$E_x\nu_{yx}=E_y\nu_{xy} \tag{2}$$

The nonlinear strain-displacement relations are

$$\varepsilon_x=u_{,x}+\frac{1}{2}(w_{,x})^2+w_{,x}w_{o,x}$$

$$\varepsilon_y=v_{,y}-w/R+\frac{1}{2}(w_{,y})^2+w_{,y}w_{o,y}$$

$$\nu_{xy}=u_{,y}+v_{,x}+w_{,x}w_{,y}+w_{,x}w_{o,y}+w_{,y}w_{o,x} \tag{3}$$

where the comma placed after a function denotes differeniation with respect to the coordinate. In equation (3), $w_o\ (x, y)$ represents the initial inward radial displacement. The total deflection is $\bar{w}$, and

$$\bar{w}=w+w_o \tag{4}$$

The equation of motion in the direction normal to the middle surface yields

$$Q_{x,x}+Q_{y,y}+(N_x\bar{w}_{,x}+N_{xy}\bar{w}_{,y})_{,x}+(N_y\bar{w}_{,y}+N_{xy}\bar{w}_{,x})_{,y}+N_y/R=\rho hw \tag{5}$$

where ρ denotes the mass density of the shell, t is the time, and $(\ )=\partial(\ )/\partial t$. In equation (5), the transverse shear forces per unit length are

$$Q_x=-(D_xw_{,xx}+D_{xy}w_{,yy})_{,x}$$

$$Q_y=-(D_{xy}w_{,xx}+D_yw_{,yy})_{,y} \tag{6}$$

and in-plane stress resultants are

$$[N_x, N_y, N_{xy}]=\int_{-h/2}^{h/2}[\sigma_x, \sigma_y, \tau_{xy}]dz \tag{7}$$

where

$$D_x=\frac{E_xh^3}{12(1-\nu_{xy}\nu_{yx})},\quad D_y=\frac{E_yh^3}{12(1-\nu_{xy}\nu_{yx})},$$

$$D_{xy}=\frac{1}{2}(D_x\nu_{yx}+D_y\nu_{xy})+2(G_{xy}h^3/12) \tag{8}$$

When body forces and in-plane inertia are neglected, the in-plane equilibrium equations are identically satisfied when the stress resultants are related to an Airy stress function $F\ (x, y, t)$ by

$$N_x=hF,yy,\quad N_y=hF,xx,\quad N_{xy}=-hF,_{xy} \tag{9}$$

The equation of motion (5) can now be written as

$$D_xw_{,xxxx}+2D_{xy}w_{,xxyy}+D_yw_{,yyyy}=h[F,_{yy}\bar{w},_{xx}+F,_{xx}(1/R+\bar{w},_{yy})-2F,_{xy}\bar{w},_{xy}]-\rho h\ w \tag{10}$$

The compatibility condition

$$\varepsilon_{x,yy}+\varepsilon_{y,xx}-\gamma_{xy,xy}=(w,_{xy})^2-(w,_{xx}w,_{yy})-\frac{1}{R}w,_{xx}+2w,_{xy}w_{o,xy}-w,_{xx}w_{o,yy}-w,_{yy}w_{o,xx} \tag{11}$$

then takes the following form:

$$F,_{xxxx}+(E_y/G_{xy}-2\nu_{yx})F,_{xxyy}+(E_y/E_x)F,_{yyyy}=E_y[(w,_{xy})^2-w,_{xx}w,_{yy}-\frac{1}{R}w,_{xx}+2w,_{xy}w_{o,xy}-w,_{xx}w_{o,yy}-w,_{yy}w_{o,xx}] \tag{12}$$

Equations (10) and (12) are the governing equations of the present analysis for the two unknown functions $w\ (x, y, t)$ and $F(x, y, t)$.

3. Modal Analysis

To solve equations (10) and (12), we use a six-term modal approximation for w, which represents the diamond-shaped buckling. This form of deflection is the same as that used by Almroth [8] for a static analysis and represents both the axisymmetric and asymmetric components of the radial reflection. The deflection function is

$$w(x, y, t)=h[a_1(t)\cos(\pi x/\lambda_x)\cos(\pi y/\lambda_y)+a_2(t)\cos(2\pi x/\lambda_x)+a_3(t)\cos(2\pi x/\lambda_x)\cos(2\pi y/\lambda_y)+a_4(t)\cos(3\pi x/\lambda_x)\cos(3\pi y/\lambda_y)+a_5(t)\cos(4\pi x/\lambda_x)+a_6(t)] \tag{13}$$

where the generalized coordinates $a_1(t)$ through $a_6(t)$ are functions of time where the generalized coordinates $a_1(t)$ through $a_6(t)$ are functions of time and λ_x and λ_y are the half-wave lengths in the axial and circumferential directions, respectively. The boundary conditions of displacements are disregarded for cylinder of moderate length.

The initial imperfection of the shell assumes the same pattern used by Nimmer and Mayers [9], namely,

$$w_o(x,y)=h[d_1\cos(\pi x/\lambda_x)\cos(\pi y/\lambda_y)+d_2\cos(2\pi x/\lambda_x)] \quad (14)$$

Substituting equations, (13) and (14) into the compatibility equation (12) leads to the following solution for F:

$$\begin{aligned}F=&[b_1\cos(7\pi x/\lambda_x)\cos(3\pi y/\lambda_y)+b_2\cos(6\pi x/\lambda_x)\cos(2\pi y/\lambda_y)+b_3\cos(5\pi/\lambda_x)\cos(3\pi y/\lambda_y)+b_4\cos(5\pi x/\lambda_x)\cos(\pi y/\lambda_y)\\&+b_5\cos(\pi x/\lambda_x)\cos(5\pi y/\lambda_y)+b^6\cos(4\pi x/\lambda_x)\cos(2\pi y/\lambda_y)+b_7\cos(2\pi x/\lambda_x)\cos(4\pi y/\lambda_y)+b_8\cos(3\pi x/\lambda_x)\cos(3\pi y/\lambda_y)\\&+b_9\cos(3\pi x/\lambda_x)\cos(\pi y/\lambda_y)+b_{10}\cos(\pi x/\lambda_x)\cos(3\pi y/\lambda_y)+b_{11}\cos(2\pi x/\lambda_x)\cos(2\pi y/\lambda_y)+b_{12}\cos(\pi x/\lambda_x)\cos(\pi y/\lambda_y)\\&+b_{13}\cos(6\pi x/\lambda_x)+b_{14}\cos(6\pi y/\lambda_y)+b_{15}\cos(4\pi x/\lambda_x)+b_{16}\cos(4\pi y/\lambda_y)\\&+b_{17}\cos(2\pi x/\lambda_x)+b_{18}\cos(2\pi y/\lambda_y)]\\&(-E_yh^2\beta^2)-\frac{1}{2}\sigma y^2+\frac{1}{2}qx^2\end{aligned} \quad (15)$$

In equation (15) σ and q represent the average axial compressive stress due to dynamic edge loading and circumferential stress, respectively. In the above equation, b_j ($j=1,\cdots,18$) are functions of $a_i(t)$, ($i=1,2,\cdots,6$), as well as geometric and material parameters. The expressions for b_j are given in the Appendix as equation (A1). The geometric and material parameters used in this study are defined as follows:

$$\alpha=\lambda_y^2/\pi^2Rh,\ \beta=\lambda_y/\lambda_x,$$

and

$$k^2=E_y/E_x,\ p^2=(E_y/G_{xy})-2\nu_{yx},\quad r^2=D_{xy}/D_x \quad (16)$$

The condition for periodic circumferential displacement v requires

$$\int_0^{2\pi R} v_{,y}dy=0$$

Using the second of equation (3), we have for the periodic condition

$$\int_0^{2\pi R}[\varepsilon_y+w/R-\frac{1}{2}(w_{,y})^2-w_{,y}w_{o,y}]dy=0$$

Applying equations (1), (7) and (9) transforms it into

$$\int_0^{2\pi R}\left[\frac{1}{E_y}(F_{,xx}-\nu_{yx}F_{,yy})+w/R-\frac{1}{2}(w_{,y})^2-w_{,y}w_{o,y}\right]dy=0 \quad (17)$$

Noticing that the functions F, w, and w_o already have periodic terms in y, we find that the condition (17) is satisfied by setting all the nonperiodic terms to zero. Therefore,

$$\bar{q}=\frac{1}{4\alpha}\left(a_1^2/2+a_1d_1+2a_3^2+\frac{9}{2}a_4^2\right)-a_6-\nu_{xy}\bar{\sigma} \quad (18)$$

where

$$\bar{q}=\frac{qR}{E_yh},\ \bar{\sigma}=\frac{\sigma R}{E_xh} \quad (19)$$

and σ and q are average stresses shown in (15).

The unit end-shortening, δ, can be obtained as follows:

$$\delta=-\frac{1}{L}\int_0^L u_{,x}dx=-\frac{1}{L}\int_0^L\left[\frac{1}{E_x}(F_{,yy}-\nu_{xy}F_{,xx})-\frac{1}{2}(w_{,x})^2-w_{,x}w_{o,x}\right]dx \quad (20)$$

The substitution of equations (13-15) into equation (20) yields

$$R\delta/h=\bar{\sigma}+\nu_{yx}\bar{q}+\frac{\beta^2}{8\alpha}\left(a_1^2+2a_1d_1+8a_2^2+16a_2d_2+4a_3^2+9a_4^2+32a_5^2\right) \quad (21)$$

We rearrange equation (10), and let

$$G(w)=\ddot{w}+\frac{D_x}{\rho h}[w_{,xxxx}+2r^2w_{,xxyy}+k^2w_{,yyyy}]-\frac{1}{\rho}[F_{,yy}\bar{w}_{,xx}+F_{,xx}(1/R+\bar{w}_{,yy})-2F_{,xy}\bar{w}_{,xy}] \quad (22)$$

where $G(w)=0$ if w and F are exact. Upon using equations (13), (14), and (15) into (10), one finds the following form:

$$\left(\frac{R^2\rho}{hE_x}\right)G(w)=\left(\frac{d^2a_1}{d\tau^2}+c_1a_1+e_1d_1+N_1\right)\phi_1+\left(\frac{d^2a_2}{d\tau^2}+c_2a_2+e_2d_2+N_2\right)\phi_2+\left(\frac{d^2a_3}{d\tau^2}+c_3a_3+N_3\right)\phi_3+\left(\frac{d^2a_4}{d\tau^2}+c_4a_4+N_4\right)\phi_4$$

$$+\left(\frac{d^2a_5}{d\tau^2}+c_5a_5+N_5\right)\phi_5+\left(\frac{d^2a_6}{d\tau^2}-k_q{}^{2}\right)\phi_6+\psi(x,y) \tag{23}$$

In the above equation, $\psi(x,y)$ is a function containing terms of the products of ϕ_i ($i=1,\ldots,6$). Define

$$\tau=(t/R)\ (E_x/\rho)^{1/2}=\text{nondimensional time} \tag{24}$$

The constants c_m ($m=1,\ldots,5$) and e_1, e_2 depend on $\bar{\sigma}$, $\bar{q}$ as well as on the geometry and material parameters. The expressions N_m are the nonlinear terms of the products of a_i and b_j, where $i=1,\ldots,6$ and $j=1,\ldots,18$. These lengthy expressions are not listed in this paper. The functions ϕ_i are:

$$\begin{aligned}
&\phi_1=\cos(\pi x/\lambda_x)\cos(\pi y/\lambda_y)\\
&\phi_2=\cos(2\pi x/\lambda_x)\\
&\phi_3=\cos(2\pi x/\lambda_x)\cos(2\pi y/\lambda_y)\\
&\phi_4=\cos(3\pi x/\lambda_x)\cos(3\pi y/\lambda_y)\\
&\phi_5=\cos(4\pi x/\lambda_x)\\
&\phi_6=1
\end{aligned} \tag{25}$$

Equation (13) can be thus written as

$$w=h\sum_{i=1}^{6}a_i(t)\phi_i$$

Galerkin's method is applied by setting

$$\int_0^L\int_0^{2\pi R}G(w)\phi_i dxdy=0 \tag{26}$$

where $i=1,\ldots,6$. The following orthogonality condition is satisfied, according to equations (23) and (25),

$$\int_0^L\int_0^{2\pi R}\psi(x,y)\phi_i dxdy=0$$

After integration, equations (26) establish six second-order nonlinear temporal differential equations for a_i ($i=1,\cdots,6$), which are generalized coordinates in deflection function w. The six equations are given in Appendix as equations (A2) through (A7).

The six temporal differential equations and the algebraic equation (18) are solved simultaneously to determine the generalized coordinates a_i ($i=1,\ldots,6$) and $\bar{q}$. The impending buckling can be determined by the observation of any sudden increase of the maximum deflecton or of the end-shortening. Numerical integration is made in accordance with the initial conditions. The solution depends upon seven parameters, namely: d_1, d_2 (the initial imperfection of the shell) in (14); α, β (the parameters governing the geometrical configuration) and p^2, k^2 (the orthotropic material properties) in (16); and $\bar{\sigma}$ (the average axial compressive stress) in (19).

4. Numerical Analysis

The set of second-order nonlinear differential equations (A2-A7) plus twelve given initial conditions defines the initial value problem of which a mathematical solution is sought. These equations have been solved numerically as functions of the five parameters (α, β, $\bar{\sigma}$, d_1, d_2) by use of the Runge-Kutta formula [10] for a cylinder made of certian kind of orthotropic material.

In order to investigate the effect of material properties on the buckling of orthotropic cylindrical shells, two orthotropic materials are selected for the numerical solutions. Calculations are also made on the isotropic cylindrical shell for the purpose of comparison. The material properties used are shown in Table 1. The dynamic buckling loads are characterized by using the stress parameter which is the ratio of the nondimensional dynamic stress and the classical static buckling stress. The stress ratio is defined as

$$\Gamma=\bar{\sigma}/\bar{\sigma}_{cL} \tag{27}$$

where $\bar{\sigma}$ is defined in (19) and $\bar{\sigma}_{cL}$ is known as the smallest critical nondimensional static axial stress in the orthotropic cylindrical shell. The criical nondimentional static axial stress for perfect orthotropic cylindrical shells is

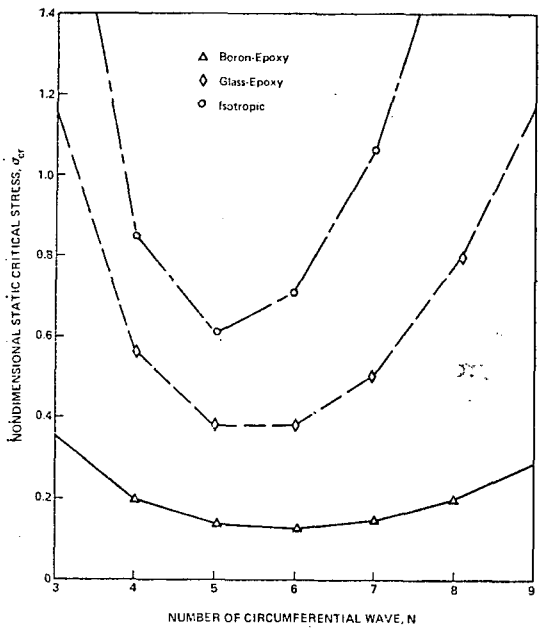

Fig. 2 Classical static buckling stress versus circumferential wave number.

denoted as $\bar{\sigma}_{cr}$, and from [11]

$$\bar{\sigma}_{cr}=\frac{\sigma_{st}R}{E_x h}=\frac{(R/h)}{m^{-2}(1-\nu_{xy}\nu_{yx})}\left\{\frac{1}{12}(h/R)^2\right.$$
$$[m^{-4}+2(\gamma^2-\nu_{yx})m^{-2}n^2+k^2n^4]$$
$$\left.+\frac{(k^2-\nu^2_{yx})m^{-4}}{m^{-4}2(k^2-\nu_{yx}\gamma^2)m^{-2}n^2/(\gamma^2-\nu_{yx})+k^2n^4}\right\} \quad (28)$$

where $\bar{m}=m\pi R/L$ and σ_{st} is the average static axial compressive stress. Figure 2 show the variation of the classical static buckling load versus circumferential wave numbers, in which the shell geometry is chosen as $R/h=100$ and $L/R=2$. From Fig. 2 one can observe that the critical circumferential wave numbers are 5 and 6 for the isotropic and glass-epoxy shells, and boron-epoxy shell, respectively. The $\bar{\sigma}_{CL}$ is the minimum value of $\bar{\sigma}_{cr}$.

Table 1 Material properties of cylindrical shells.

	Glass-epoxy	Boron-epoxy	Isotropic (Steel)
E_x N/m² (psi)	5.17×10^{10} (7.5×10^6)	27.58×10^{10} (40×10^6)	20.69×10^{10} (30×10^6)
E_y N/m² (psi)	2.41×10^{10} (3.5×10^6)	3.103×10^{10} (4.5×10^6)	20.69×10^{10} (30×10^6)
G_{xy} N/m² (psi)	0.86×10^{10} (1.25×10^6)	1.034×10^{10} (1.5×10^6)	7.959×10^{10} (11.54×10^6)
ν_{xy}	0.25	0.25	0.30
ν_{yx}	0.1167	0.0281	0.30
k^2	0.4667	0.1125	1.0
γ^2	0.4403	0.1026	1.0
p^2	2.5666	2.9438	2.0

5. Buckling Criterion

The dynamic buckling load is determined when that load causes a distinctly large rise of the peak amplitude of the deflection [5]. The same phenomena are observed on the end-shortening of the shell in the present analysis. Typical variations of the unit end-shortening and the maximum amplitude of a_1 with the axial stress in a boron-epoxy cylinder are shown in Figure 3, from which one can see that the jumps of end-shortening and ma-

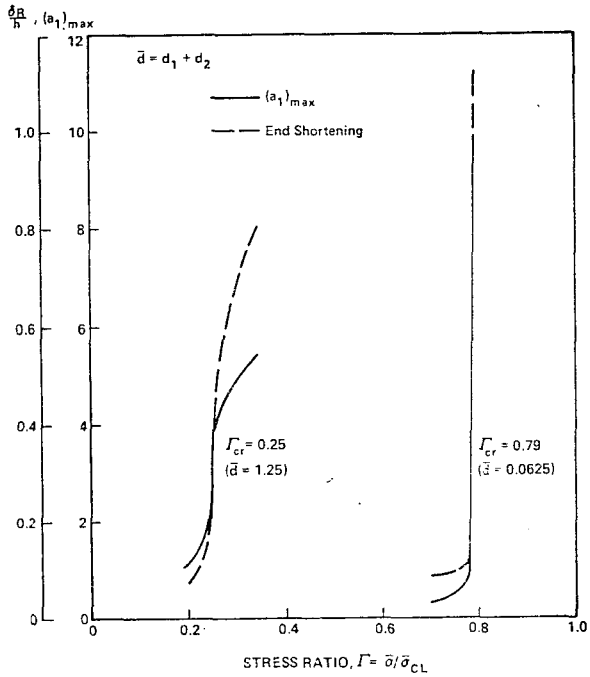

Fig. 3 Variations of the unit end-shortening $\frac{\delta R}{h}$ and first generalized coordinate $(a_1)_{max}$ with stress ratio Γ.

ximum amplitude occur at the same load. In this study the a_1 mode is used for determining the dynamic buckling stress, $\bar{\sigma}_b$, which is the critical value of $\bar{\sigma}$ defined in (19). The relative imprefection amplitudes are chosen as $d_1=4d_2$ [9]. The imperfection parameter $\bar{d}$ is defined as $\bar{d}=d_1+d_2$. The critical stress ratio, Γ_{cr}, is the ratio of $\bar{\sigma}_b/\sigma_{cL}$.

Buckling Mode

The actual buckling mode of a cylindrical shell under axial compression cannot be represented exactly with several finite integer numbers of axial and circumferential waves. In this study the geometrical parameters α and β are used for mode shapes of a cylindrical shell under step loads. The geometrical parameters α and β are related to the wave lengths such as

$$\alpha=R/(n^2h),\quad \beta=2(m\pi R/nL) \tag{29}$$

For determining the dynamic buckling load, the minimum critical load is determined by numerical results over a range of α and β. If one assumes that the classical static buckling mode can be used as a starting point in the numerical calculations, then the ranges of α and β in the present study give

$$2.77<\alpha<4.0 \text{ and } 0.5236<\beta<0.6283.$$

Typical results of this study are shown in Figure 4 with the initial imperfections, $d_1=1.0$ and $d_2=0.25$. From Figure 4 the critical geometric parameter α, which is related to the shell thickness and the number of circumferential waves, can be represented with 3.0. However, the parameter β (29) can vary between 0.4 and 0.6 according to the material properties of the shell.

Dynamic Buckling Load

The dynamic buckling load of a perfect isotropic cylindrical shell under axial step load is generally higher than the classical static bucking load of that shell. However, the dynamic buckling load of a perfect orthotropic cylindrical shell under axialp step load is lower than the classical static buckling load of the same cylindrical shell. In Figure 5, the variations of buckling stress ratio with initial imperfections are shown. In that figure, the dynamic buckling stress ratio Γ_{cr} decreases with decreasing value of elastic constant ratio, $\frac{E_y}{E_x}$, as shown n Table 2. In that table $(\sigma_b)_0$ is biuckling stress in a perfect cylinder. The decreasing phenomena of the

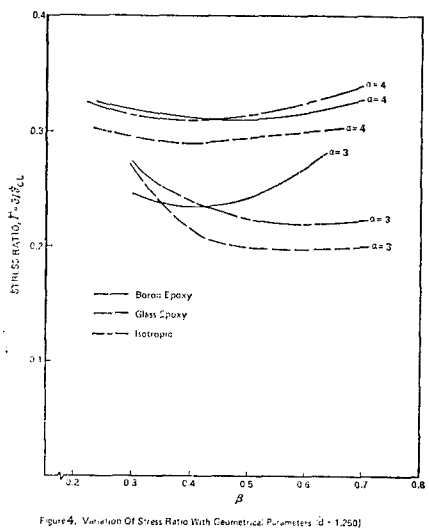

Figure 4. Variation Of Stress Ratio With Geometrical Parameters ($\bar{d}$ = 1.250)

Fig. 4 Variation of stress ratio with geometrical parameters ($\bar{d}=1.250$).

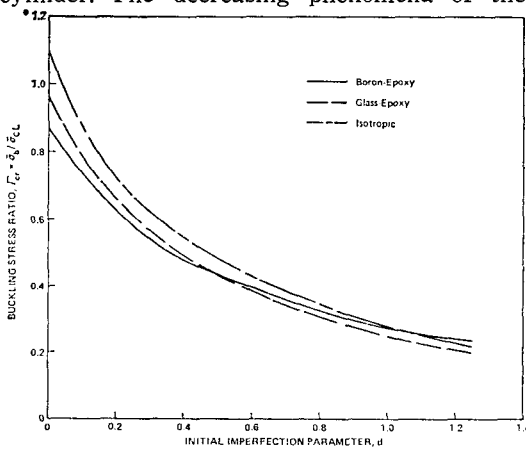

Figure 5. Variations Of Dynamic Buckling Stress With Initial Imperfections

Fig. 5 Variations of dynamic buckling stress with initial impertections.

dynamic buckling stress parameter may be related to the stress wave speed. Unlike the isotropic shell, the orthotropic cylindrical shells have wave propagation velocities smaller in the circumferential direction than that in the axial direction. This difference of axial and circumferential wave propagation velocities may cause the weakening of resistance to the buckling. Zimcik and Tennyson [7] showed that the responses of anisotropic cylindrical shell subjected to the axial impulsive loading based on the theories of buckling analysis and stress wave analysis were similar. Thus, one can expect that the dynamic buckling load of the shells is sensitive to the orthotropic materials properties.

Table 2 Dynamic buckling stress of perfect orthotropic cylindrical shells under axial step load.

Material	$(\Gamma_{cr})_0=(\bar{\sigma}_{b0})/\bar{\sigma}_{cL}$	$k^2=E_y/E_x$
Boron-epoxy	0.87	0.1125
Glass-epoxy	0.97	0.4667
Isotropic	1.10	1.0000

Initial Imperfection

The ratio of critical axial loads on an imperfect cylinder and on a perfect cylinder is expressed as

$$\overline{P}=\bar{\sigma}_b/\sigma_{b0} \qquad (30)$$

where $\bar{\sigma}_{b0}$ is the dynamic buckling stress of a perfect cylinder. The initial imperfection of an orthotropic cylindrical shell under axial step load plays a dominant role in the reduction of dynamic buckling load as shown in Fig. 6. One can also see that the smaller values of $\frac{E_y}{E_x}$ of the shell lead less imperfection sensitivity. Similar results are observed in static buckling analysis [3]. Table 3 shows the influence of initial imperfection on the dynamic buckling stress $\bar{\sigma}_b$.

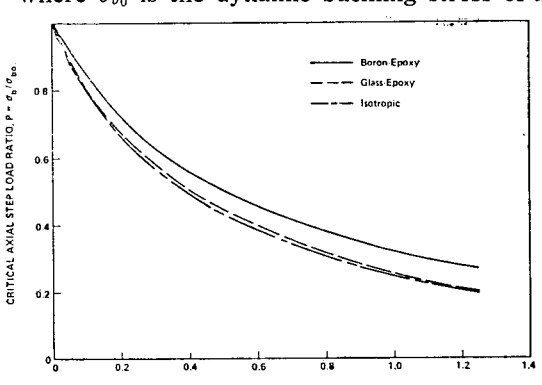

Fig. 6 Effect of initial imperfection on the critical axil load.

Table 3 The buckling stress ratio versus initial imprefection.

Initial imperfection parameter, $\bar{d}=d_1+d_2$	Materials	α	β	$\Gamma_{cr}=\bar{\sigma}_b/\sigma_{cL}$
1.25	Boron-epoxy	3.0	0.4	0.247
	Glass-epoxy	3.0	0.55	0.198
	Isotropic	3.0	0.6	0.220
0.625	Boron-epoxy	3.0	0.5	0.385
	Glass-epoxy	3.0	0.5	0.375
	Isotropic	3.0	0.5	0.420
0.375	Boron-epoxy	3.0	0.5	0.498
	Glass-epoxy	3.0	0.5	0.510
	Isotropic	3.0	0.5	0.573
0.125	Boron-epoxy	3.0	0.5	0.698
	Glass-epoxy	3.0	0.5	0.745
	Isotropic	3.0	0.5	0.835
0.0625	Boron-epoxy	3.0	0.5	0.785
	Glass-epoxy	3.0	0.5	0.847
	Isotropic	3.0	0.5	0.950
0 (perfect)	Boron-epoxy	3.0	0.5	0.870
	Glass-epoxy	3.0	0.5	0.970
	Isotropic	3.0	0.5	1.100

6. Conclusion

The six-term deflection function was used for the analysis of dynamic buckling of orthotropic cylindrical shells under axial step loads. This approximate deflection function represents dynamic behavior of the cylindrical shell agreeable with experimental results [7] at least for the perfect and isotropic case. The buckling

mode shape are found to vary with the initial imperfections and the material properties of the shells. The dynamic buckling stress is significantly reduced due to the initial imperfections. The imperfection sensitivity of an orthotropic cylindrical shell is lower than that of the isotropic cylindrical shell.

References

1. von Karman, Th. and Tsien, H.S., "The Buckling of Thin Cylindrical Shells under Axial Compression," Journal of Aeronautical Science, Vol. 8, August 1941, pp. 303-212.
2. Donnell, L.H. and Wan C.C., "Effects of Imperfections on Buckling of Thin Cylinders and Columns under Axial Compression," Journal of Applied Mechanics, Trans. of ASME, Series E, Vol. 17, No. 1, Mar. 1950, pp. 73-83.
3. Khot, N.S., "Postbuckling Behavior of Geometrically Imperfect Composite Cylindrical Shells Under Axial Compression," AIAA Journal Vol. 8, No. 3, March 1970, pp. 579-581.
4. Booton, N. and Tennyson, R.C., "Buckling of Imperfect Anisotropic Circular Cylinders under Combined Loading," AIAA Journal Vol. 17, No. 3, March 1979, pp. 278-287.
5. Roth, R.S. and Klosner, J.M., "Nonlinear Response of Cylindrical Shells Subjected to Dynamic Axial Loads," AIAA Journal, Vol. 2, No. 10, Oct. 1964, pp. 1788-1794.
6. Tamura, Y.S. and Babcock, C.D., "Dynamic Stablity of Cylindrical Shells Under Step Loading," Journal of Applied Mechanics Trans. of ASME, Series E, Vol. 42, No. 1, March 1975, pp. 190-194.
7. Zimcik, D.G., and Tennyson, R.C., "Stability of Circular Cylindrical Shells under Transient Axial Impulsive Loading," AIAA Journal, Vol. 18, No. 6, June 1980, pp. 691-199.
8. Almroth, B.O., "Postbuckling Behavior of Orthotropic Cylinder under Axial Compression," AIAA Journal, Vol. 2, No. 10, Oct. 1964, pp. 1795-1799.
9. Nimmer, R. P. and Mayers, J., "Limit Point Buckling Loads of Axially Compressed, Circular Cylindrical Shells-The Effect of Nonlinear Material Behavior," Journal of Applied Mechanics. Trans. of ASME, Series E. Vol. 46, No. 2, June 1979, pp. 386-392.
10. James, M.L., Smith, G.M., and Wolford, J.C., Applied Numerical Methods for Digital Computation, Second Edition, Harper & Row, Publishers, New York, N.Y., 1977, p. 410.
11. Brush, D.O., and Almroth, B.O., Buckling of Bars, Plates, and Shells, McGraw-Hill Book Co., 1975, p. 180.

APPENDIX

$$b_1=\frac{72a_4a_5}{(7^4\beta^4+21^2p^2\beta^2+3^4k^2)},$$

$$b_2=\frac{32a_3a_5}{(6^4\beta^4+144p^2\beta^2+16k^2)},$$

$$b_3=\frac{18(a_2a_4+a_4d_2)}{(5^4\beta^4+225p^2\beta^2+81k^2)},$$

$$b_4=\frac{4(2a_1a_5+9a_3a_4+2a_5d_1)}{(5_4\beta^4+25p^2\beta^2+k^2)},$$

$$b_5=\frac{36a_3a_4}{(\beta_4+25p^2\beta^2+5^4k^2)},$$

$$b_6=\frac{9(a_1a_4+a_4d_1)+8(a_2a_3+a_3d_2)}{(4^4\beta^4+64p^2\beta^2+16k^2)}, \qquad \text{(A1)}$$

$$b^7=\frac{9(a_1a_4+a_4d_1)}{(16\beta^4+64p^2\beta^2+4^4k^2)},$$

$$b^8=\frac{9\alpha a_4}{(81\beta^4+81p^2\beta^2+81k^2)},$$

$$b^9=\frac{2(2a_1a_3+a_1a_2+a_1d_2+a_2d_1+4a_1a_5+2a_3d_1+4a_5d_1)}{(81\beta^4+9p^2\beta^2+k^2)}$$

$$b_{10}=\frac{2(2a_1a_3+9a_2a_4+2a_3d_1+36a_4a_5+9a_4d_2)}{(\beta^4+9p^2\beta^2+81k^2)}$$

$$b_{11}=\frac{8a_3a_5-\alpha a_3}{4(\beta^4+p^2\beta^2+k^2)},$$

$$b_{12}=\frac{2a_1a_2+2a_1d_2+2a_2d_1-\alpha a_1}{(\beta^4+p^2\beta^2+k^2)},\quad b_{13}=\frac{a_4{}^2}{32\beta^4},$$

$$b_{14}=\frac{a_4{}^2}{32k^2},\quad b_{15}=\frac{(a_3{}^2-2\alpha a_5)}{32\beta^4},\quad b_{16}=\frac{a_3{}^2}{32k^2}$$

$$b_{17}=\frac{(a_1{}^2+2a_1d_1-8\alpha a_2)}{32\beta^4},$$

$$b_{18}=\frac{(a_1{}^2+2a_1d_1+16a_2a_3+16a_3d_2)}{32k^2}$$

$$\frac{d^2a_1}{d\tau^2}+\frac{A_1}{12a_1}-\frac{\beta^2\bar{\sigma}}{\alpha}(a_1+d_1)+[2B_1(a_1+d_1)(a_1{}^2$$

$$+2a_1d_1-8\alpha a_2)+2B_2(a_1+d_1)(a_1^2+2a_1d_1+16a_2a_3+16a_3d_2)+4B_3(a_2+d_2)(a_1a_2+2a_1a_3+a_1d_2+a_2d_1+4a_1a_5+2a_3d_1+4a_5d_1)+4B_4(a_2+d_2)(a_1a_2+a_1d_2+a_2d_1-\alpha a_1/2)+8B_3a_3(2a_1a_3+a_1a_2+a_1d_2+a_2d_1+4a_1a_5+2a_3d_1+4a_5d_1)+8B_5a_3(2a_1a_3+9a_2a_4+2a_3d_1+36a_4a_5+9a_4d_2)+9B_6a_4(9a_1a_4+8a_2a_3+8a_3d_2+9a_4d_1)+81B_7a_4(a_1a_4+a_4d_1)+32B_8a_5(2a_1a_5+9a_3a_4+2a_5d_1)+16B_3a_5(a_1a_2+2a_1a_3+4a_1a_5+a_1d_2+a_2d_1+2a_3d_1+4a_5d_1)-2\alpha\beta_4(a_1a_2+a_1d_2+a_2d_1-\alpha a_1/2)](k^2\beta^4/\alpha^2)+\frac{k^2}{\alpha}(a_1+d_1)\bar{q}=0 \quad (A2)$$

$$\frac{d^2a_2}{d\tau^2}+\frac{4}{3}A_2a_2-\frac{4\beta^{2-}\bar{\sigma}}{\alpha}(a_2+d_2)+[2B_3(a_1a_2+2a_1a_3+4a_1a_5+a_1d_2+a_2d_1+2a_3d_1+4a_5d_1)(a_1+d_1)+2B_4(a_1+d_1)(a_1a_2+a_1d_2+a_2d_1-\alpha a_1/2)+4B_6a_3(9a_1a_4+8a_2a_3+8a_3d_2+9a_4d_1)+8B_2a_3(a_1^2+2a_1d_1+16a_2a_3+16a_3d_2)+162B_9a_4(a_2a_4+a_4d_2)+18B_5a_4(2a_1a_3+9a_2a_4+2a_3d_1+36a_4a_5+9a_4d_2)-4\alpha B_1(a_1^2+2a_1d_1-8\alpha a_2)](k^2\beta^4/\alpha^2)=0 \quad (A3)$$

$$\frac{d^2a_3}{d\tau^2}+\frac{4}{3}A_1a_3-\frac{4\beta^{2-}\bar{\sigma}}{\alpha}a_3+[8B_3(a_1+d_1)(a_1a_2+2a_1a_3+4a_1a_5+a_1d_2+a_2d_1+2a_3d_1+4a_5d_1)+8B_5(a_1+d_1)(2a_1a_3+9a_2a_4+2a_3d_1+36a_4a_5+9a_4d_2)+8B_6(a_2+d_2)(9a_1a_4+8a_2a_3+8a_3d_2+9a_4d^1)+16B_2(a_2+d_2)(a_1^2+2a_1d_1+16a_2a_3+16a_3d_2)+32B_1(a_3^3-2\alpha a_3a_5)+32B_2a_3^3+144B_8a_4(2a_1a_5+9a_3a_4+2a_5d_1)+1296B_{10}a_3a_4^2+64B_3a_3a_5^2+B_4(8a_3a_5-\alpha a_3)(8a_5-\alpha)](k^2\beta^4/\alpha^2)+\frac{4k^2q}{\alpha}a_3=0 \quad (A4)$$

$$\frac{d^2a_4}{d\tau^2}+\frac{27}{4}A_1a_4-\frac{9\beta^{2-}\bar{\sigma}}{\alpha}a_4+[162(B_1+B_2)a_4^3+9B_6(a_1+d_1)(9a_1a_4+8a_2a_3+8a_3d_2+9a_4d_1)+81B_7(a_1+d_1)(a_1a_4+a_4d_1)+324B_9(a_2+d_2)(a_2a_4+a_4d_2)+36B_5(a_2+d_2)(2a_1a_3+9a_2a_4+2a_3d_1+36a_4a_59a_4d_2)+144B_8a_3(2a_1a_5+9a_3a_4+2a_5d_1)+1299B_{10}a_3^2a_4+5184B_{11}a_4a_5^2+144B_5a_5(2a_1a_3+9a_2a_4+2a_3d_1+36a_4a_5+9a_4d_2)-\alpha^2B_4a_4](k^2\beta^4/\alpha^2)+\frac{9k^{2-}q}{\alpha}a_4=0 \quad (A5)$$

$$\frac{d^2a_5}{d\tau^2}+\frac{64}{3}A_2a_5-\frac{16\beta^{2-}\sigma}{\alpha}a_5+16B_8(a_1+d_1)(2a_1a_5+9a_3a_4+2a_5d_1)+8B_3(a_1+d_1)(a_1a_2+2a_1a_3+4a_1a_5+a_1d_2+a_2d_1+2a_3d_1+4a_5d_1)+32B_3a_3^2a_5+4B_4(8a_3^2a_5-\alpha a_3^2)+2592B_{11}a_4^2a_5+72B_5a_4(2a_1a_3+9a_2a_4+2a_3d_1+36a_4a_5+9a_4d_2-160B_1(a_3^2-2\alpha a_5)](k^2\beta^4/\alpha^2)=0 \quad (A6)$$

$$\frac{d^2a_6}{d\tau^2}-k^{2-}q=0 \quad (A7)$$

In the above equations,

$$A_1=\frac{\beta^4+2[\nu_{yx}+2G_{xy}/E_x(1-\nu_{xy}\nu_{yx})]\beta^2+k^2}{\alpha^2(1-\nu_{xy}\nu_{yx})}$$

$$A_2=\frac{\beta^4}{\alpha^2(1-\nu_{xy}\nu_{yx})},\quad B_1=\frac{1}{32\beta^4}$$

$$B_2=\frac{1}{k^2},\quad B_3=\frac{1}{81\beta^4+9p^2\beta^2+k^2}$$

$$B_4=\frac{1}{\beta^4+p^2\beta^2+k^2},\quad B_5=\frac{1}{\beta_4+9p^2\beta^2+81k^2}$$

$$B_6=\frac{1}{256\beta^4+64p^2\beta^2+16k^2}$$

$$B_7=\frac{1}{16\beta^4+64p^2\beta^2+256k^2}$$

$$B_8=\frac{1}{625\beta^4+25p^2\beta^2+k^2}$$

$$B_9=\frac{1}{625\beta^4+225p^2\beta^2+81k^2}$$

$$B_{10}=\frac{1}{\beta_4+25p^2\beta^2+625k^2}$$

$$B_{11}=\frac{1}{2401\beta^4+441p^2\beta^2+81k^2}$$